MOCVD Growth of β-Ga_2O_3 with Fast Growth Rates (> 4.3 μm/h), Low Controllable Doping and Superior Transport Properties

Dong Su Yu[1,*], Lingyu Meng[1,*], and Hongping Zhao[1, 2, †]

[1]*Department of Electrical and Computer Engineering, The Ohio State University, Columbus, OH 43210, USA*

[2]*Department of Materials Science and Engineering, The Ohio State University, Columbus, OH 43210, USA*

* Equally Contributed First-Authorship

[†]Corresponding author Email: zhao.2592@osu.edu

Abstract

Si-doped β-phase (010) Ga_2O_3 epi-films with fast growth rates were comprehensively investigated using trimethylgallium (TMGa) as the Ga precursor via metalorganic chemical vapor deposition (MOCVD). Two main challenges facing in MOCVD growth of thick (010) β-Ga_2O_3 films with fast growth rates include high impurity carbon (C) incorporation and rough surface morphologies due to the formation of imbedded 3D pyramid-shaped structures. In this work, two different categories of oxygen source (high purity O_2 > 99.9999% and O_2^* with 10 ppm of [H_2O]) were used for β-Ga_2O_3 MOCVD growth. Our study revealed that the size and density of the 3D defects in the β-Ga_2O_3 epi-films were significantly reduced when the O_2^* was used. In addition, the use of off-axis (010) Ga_2O_3 substrates with 2° off-cut angle leads to further reduction of defects formation in β-Ga_2O_3 with fast growth rates. To suppress C incorporation in MOCVD β-Ga_2O_3 grown with high TMGa flow rates, our findings indicate that high O_2 (or O_2^*) flow rates are essential. Superior room temperature electron mobilities as high as 110-190 $cm^2/V{\cdot}s$ were achieved for β-Ga_2O_3 grown using O_2^* (2000 sccm) with a growth rate of 4.5 μm/h (film thickness of 6.3 μm) within the doping range of 1.3 x10^{18}-7 x10^{15} cm^{-3}. The C incorporation is significantly suppressed from ~10^{18} cm^{-3} to <5 x10^{16} cm^{-3} ([C] detection limit) for β-Ga_2O_3 grown using high O_2 (O_2^*) flow rate of

2000 sccm. Results from this work will provide guidance on developing high quality thick β-Ga_2O_3 films required for high power electronic devices with vertical configurations.

Keywords: MOCVD β-Ga_2O_3, fast growth rate, electron transport properties, off-axis substrates

Among the five polymorphs of gallium oxide (Ga_2O_3) — α (corundum), β (monoclinic), γ (defective spinel) , δ (orthorhombic) , and ε (orthorhombic) — the β-phase Ga_2O_3 is the most thermally and chemically stable one.[1-3] β-Ga_2O_3 represents a promising semiconductor material for power electronics because of its ultra-wide bandgap (UWBG) of ~4.8 eV and predicted critical electric field strength of 8 MV/cm.[4-6] Despite its UWBG, a wide n-type doping range between 10^{16} – 10^{20} cm^{-3}, and peak room temperature electron mobility of ~200 cm^2/Vs that is close to the theoretical predicted limit have been experimentally demonstrated.[7-13] Among several UWBG semiconductor candidates such as AlN, diamond, and BN, β-Ga_2O_3 has its unique advantage of the availability of high-quality bulk Ga_2O_3 synthesized with low density of defects from melt growth techniques.[14-19] The availability of high quality β-Ga_2O_3 epitaxy films grown on native Ga_2O_3 substrates with effective and controllable n-type doping promise its applications in transistors[20-23], Schottky barrier diodes[14-27] and ultra-violet (UV) solar-blind photodetectors[28-29].

High quality β-Ga_2O_3 thin film growths have been investigated via various techniques such as molecular beam epitaxy (MBE)[21, 30-33], low-pressure chemical vapor deposition (LPCVD)[34-37], pulsed laser deposition (PLD)[38-40], halide vapor phase epitaxy (HVPE)[8,41-42], and metalorganic chemical vapor deposition (MOCVD)[11-12,43-49]. HVPE provides fast growth rates (>5 μm/h), facilitating the efficient deposition of thick β-Ga_2O_3 films. Thus far, the majority of vertical β-Ga_2O_3 Schottky barrier diodes and p-n junction diodes are presently fabricated using HVPE grown thick drift layers.[50-54] However, due to the associated rough surface morphologies, HVPE grown

films require a chemical-mechanical polishing (CMP) process to achieve smooth surface prior device fabrication.[55] The MOCVD grown β-Ga_2O_3 thin films have shown promising material properties such as wide n-type doping range with superior electron mobilities, smooth surface morphology, and tunable growth rate range. Consequently, MOCVD is considered as a scalable growth method for developing device quality epitaxial films. Recently, the use of TMGa as the Ga precursor in the MOCVD growth of the β-Ga_2O_3 epitaxial films on (010) β-Ga_2O_3 substrate has been successfully demonstrated with fast growth rates up to 3 μm/h and high electron mobilities up to 190 cm^2/Vs.[7] Previous studies on β-Ga_2O_3 MOCVD growth using TMGa in a close-coupled showerhead reactor have shown fast growth rates reaching up to 9.8 μm/h.[56] Additionally, MOCVD growth of (010) β-Ga_2O_3 films using TMGa at a growth rate of 1.5 μm/h achieved a room temperature Hall mobility of 125 $cm^2/V{\cdot}s$ and a peak mobility of 23000 $cm^2/V{\cdot}s$ (at 32 K).[11, 13, 57] These findings suggest significant potential for the growth of thick and high-quality β-Ga_2O_3 epi-films via MOCVD by using TMGa as the Ga precursor. TMGa (65 Torr at 0 ℃) exhibits a higher vapor pressure than TEGa (3 Torr at 20 ℃), which ensures its suitability for developing MOCVD growth of thick β-Ga_2O_3 films with fast growth rates. Moreover, TMGa decomposes thermally in a two-step process, while TEGa undergoes a three-step decomposition (β-elimination). The shorter reaction pathway also enables faster growth rates of β-Ga_2O_3 films with TMGa.[57-59] However, as the growth rate increases, the surface quality of β-Ga_2O_3 films degrades due to the formation of 3D pyramid-shaped defective structures associated with the fast growth rate conditions. Another challenge is that the incorporation of C impurity in MOCVD growth of β-Ga_2O_3 films increases with the increase of TMGa molar flow rate or growth rate. The role of C in β-Ga_2O_3 is rather complex. When C occupies the Ga site, it serves as a shallow donor, which is often passivated by H. When C occupies the O site, it serves as a compensation center.[60-61]

Prior studies on MOCVD homoepitaxy of (100) β-Ga_2O_3 on the on-axis substrates revealed the formation of stacking faults and twin lamellae.[62] By introducing appropriate off-cut angles on the (100) substrates, step-flow growth of β-Ga_2O_3 thin films on (100) plane were achieved,[63-68] indicating the benefits of using off-axis substrates to improve β-Ga_2O_3 crystalline quality.

In this work, comprehensive studies of MOCVD growth of β-Ga_2O_3 films using high purity O_2 (> 99.9999 %) or O_2^*(with 10 ppm of [H_2O]) on both on-axis and 2º off- axis (010) β-Ga_2O_3 substrates were performed using TMGa as Ga precursor. The primary objective of this study is to achieve MOCVD growth of high crystalline quality (010) β-Ga_2O_3 films with fast growth rates, low C incorporation, and smooth surface morphologies. Our studies show that the use of O_2^* can significantly improve surface smoothness, particularly for films grown at relatively fast growth rates. Incorporation of off-axis (010) Ga_2O_3 substrates also facilitates the growth of films with smooth surface morphologies. High group VI/III ratio with high O_2 or O_2^* flow rates can effectively suppress background C incorporation. Results from this work will advance the development of MOCVD β-Ga_2O_3 films for high power electronics.

β-Ga_2O_3 films were grown on commercial semi-insulating (010) Fe-doped β-Ga_2O_3 substrates using Agnitron's Agilis 100 MOCVD reactor. Ga_2O_3 substrates with both on-axis and 2º off-cut angle (from Novel Crystal Technology, Inc.) were used in this study. The 2º off-cut angle substrate is cut at an angle of 2º in the [001] direction. The substrates were cleaned using acetone, isopropyl alcohol (IPA), and de-ionized (DI) water before being loaded into the growth chamber. TMGa was used as the Ga precursor, and O_2 or O_2^* was used as the O precursor. O_2^* comes from a gas cylinder containing a mixture of H_2O and O_2. Argon (Ar) was used as the carrier gas with flow rates ranging between 400 standard cubic centimeters per minute (sccm) and 1100 sccm. The growth temperature and growth pressure were maintained at 950 ℃ and 60 Torr, respectively. Si-

doped β-Ga_2O_3 films were grown at growth rate ranging from 4.3 μm/h to 8.1 μm/h by controlling the TMGa molar flow rate from 87 μmol/min to 116 μmol/min and the O_2 (or O_2^*) flow rate from 800 sccm to 2000 sccm. The total thickness of the β-Ga_2O_3 films varied with the growth rate and growth duration, reaching up to 9.6 μm. The diluted silane (SiH_4) molar flow rate was adjusted from 0.03 nmol/min to 40 nmol/min to achieve a low to high n-type doping range. To characterize the quality of the surface morphologies and the surface roughness of the β-Ga_2O_3 films, optical microscopy, field emission scanning electron microscopy (FESEM, FEI Helios 650), and atomic force microscopy (AFM, Bruker AXS Dimension Icon 3) were employed. The film thicknesses were estimated by examining the SEM cross-sectional views of samples grown on co-loaded c-sapphire substrates. Ti/Au (30/100 nm) were deposited at the four corners of each sample to form ohmic contacts, and the Hall measurements were conducted using the van der Pauw Hall measurement (Ecopia HMS 3000). Quantitative secondary-ion mass spectrometry (SIMS) was performed to probe the impurity profiles of C, H, and Si in the designed SIMS sample which contains sublayers that were grown with various MOCVD growth conditions.

β-Ga_2O_3 films were grown on two different types of substrates (on-axis and 2º off-cut β-Ga_2O_3) using O_2 (or O_2^*) at a growth rate ranging from 4.3 μm/h to 8.1 μm/h by systematically adjusting the TMGa molar flow rate between 87 μmol/min and 116 μmol/min, along with tuning the O_2 (or O_2^*) flow rate from 800 sccm to 2000 sccm. Detailed growth conditions and the corresponding characteristics of the β-Ga_2O_3 films grown on on-axis (010) Fe-doped β-Ga_2O_3 substrates are listed in Table 1. Figure 1 compares the surface morphologies of β-Ga_2O_3 films (samples #2 and #11) grown using two different types of O_2 sources: O_2 vs. O_2^*. Both films were grown on the on-axis (010) Fe-doped β-Ga_2O_3 substrates at a growth rate of 4.5 μm/h with a total thickness of 6.3 μm. From the optical microscopy and FESEM imaging, the size and density of the

3D pyramid-shaped defects in the β-Ga_2O_3 film grown with O_2* are smaller and less dense than those in the film grown using O_2. Note that for the samples grown using O_2*, a relatively high density of surface structures with much smaller feature sizes was observed. The distribution of these surface structures was highly uniform across the entire sample surface. The incorporation of H_2O during the growth process enhances the smoothness of Ga_2O_3 film surfaces by improving surface kinetics and diffusion dynamics. Previous studies have indicated that when H_2O molecules dissociate, it generates a significantly higher concentration of hydrogen as compared to the pure oxygen.[69] The increase in H concentration positively impacts the kinetic conditions on the substrate surface, enhancing adatom mobility and increasing the diffusion length of the adatoms. Wagner et al. has also demonstrated the introducing H_2O facilitates layer-by-layer growth, leading to smoother and more uniform film surfaces.[70] Additionally, the RMS value of the β-Ga_2O_3 film grown with O_2* was lower at 1.48 nm compared to 2.59 nm for the β-Ga_2O_3 film grown using O_2. Under the same growth conditions, the surface morphology of the sample grown with O_2* (sample #11) showed significant improvement as compared to the sample grown with O_2 (sample #2). Note that similar electron mobilities were measured between these two samples. As the film thickness reduces, one should expect more prominent influence of the surface or interface roughness on the transport properties. Future investigation is still required to understand the impact of the surface morphology on device performance. In particular, for devices with thick epitaxial layers, additional optimization of surface morphology may still be necessary.

To investigate the impact of the use of off-axis substrates on the film quality and film morphology, several β-Ga_2O_3 films were grown on (010) Fe-doped β-Ga_2O_3 substrates with a 2º off-cut angle. The growth conditions of the samples grown on 2º off-cut substrates were listed in Table 2. The TMGa molar flow rate was adjusted from 87 μmol/min to 116 μmol/min, and the O_2

(or O_2^*) flow rate was tuned from 800 sccm to 2000 sccm. Correspondingly, the film growth rate achieved ranged from 4.3 μm/h to 8.1 μm/h. Figure 2 shows the optical microscopy, SEM, and AFM images, respectively, illustrating the surface morphologies and corresponding RMS roughness values of the β-Ga_2O_3 samples grown on two different types of substrates (on-axis and 2º off-cut) under different growth conditions. The surface morphologies of the β-Ga_2O_3 samples grown using O_2 with 7 μm/h growth rate and 308 VI/III ratio on the on-axis and 2º off-cut angle (010) β-Ga_2O_3 substrate were shown in Figure 2(a), (g), (m) (sample #1), and (b), (h), (n) (sample #14), respectively. From the comparison, the size and density of the surface defects on sample #14 are much suppressed as compared to those of sample #1.

From a different set of comparison, in which the samples were grown with O_2^*, growth rate of 8.1 μm/h, and VI/III ratio of 385, sample #4 (Figure 2(c), (i), (o)) was grown on on-axis substrate and sample #15 (Figure 2(d), (j), (p)) was grown on 2º off-cut substrate. It was observed that the surface morphology of sample #15 is much smoother as compared that of sample #4. For the case of films grown with increased VI/III ratio of 1026, reduced growth rate of 4.3 μm/h using O_2^*, and total film thickness of 9.6 μm, the surface morphology of sample #16 (Figure 2(f), (l), (r)) grown on 2º off-cut substrate has a minimum density of defects as compared to that of sample #13 (Figure 2(e), (k), (q)), which was grown on on-axis substrate. From the comparison as shown in Fig. 2, films grown on 2º off-cut substrates show significant improvement of the surface smoothness with reduced density of defects. The introduction of off-cut angle on β-Ga_2O_3 substrates provides preferred nucleation sites for incoming Ga adatoms along the steps/edges, which suppresses the random nucleation sites and the formation of 3D defects. Furthermore, the use of O_2^* and relatively high VI/III ratio result in optimal surface smoothness.

Figure 3 shows the optical microscopy, FESEM, and AFM images of β-Ga_2O_3 films (samples #3, #4, #6, and #7) grown under different VI/III ratios. With a fixed TMGa molar flow rate of 116 μmol/min, as the VI/III ratio increases from 308 (sample #3, Fig. 3(a, e, i)), to 385 (sample #4, Fig. 3(b, f, j)) and 1155 (sample #6, Fig. 3(c, g, k)), the overall surface smoothness improves with reduced density of 3D pyramid-shaped structure defects. In addition, the β-Ga_2O_3 film grown with a comparatively lower TMGa molar flow rate of 87 μmol/min and a corresponding slower growth rate (4.5 μm/h) as shown in Fig. 3(d, h, l), achieved excellent surface morphology with minimum surface density of defects. This film was grown at a VI/III ratio of 1026. From this study, the use of a higher VI/III ratio is advantageous for enhancing the smoothness of the β-Ga_2O_3 surface morphology, especially at increased growth rates. Additionally, the films grown with the TMGa molar flow rate of 116 μmol/min showed a trend of decreasing RMS values correlating with higher VI/III ratios (Fig. 3(i, j, k)).

For the MOCVD growth of β-Ga_2O_3 films using TMGa as the Ga precursor, it has previously shown that films grown with fast growth rates experience severe charge compensation due to increased C incorporation.[53] Here, with an expanded growth window, the background C and H incorporation were quantitatively probed. Figure 4(a) shows the schematic of a multi-layer stack sample designed for in-depth SIMS characterization for [C], [Si] and [H] in β-Ga_2O_3 sub-layers grown with different growth conditions.

The SIMS sample was grown under two different categories of oxygen (O_2 vs. O_2^*), with oxygen flow rate set at 800, 1500, and 2000 sccm. The TMGa molar flow rate and growth temperature was fixed at 87 μmol/min and 950 °C, respectively. As shown in Figure 4(b), quantitative SIMS analysis reveals that increased O_2 (or O_2^*) flow rate substantially reduced C incorporation. In the sub-layers subjected to O_2 (or O_2^*) flow rate of 1500 and 2000 sccm, the C

concentration was suppressed to the detection limit of 5 x10^{16} cm^{-3}. The carbon level was relatively higher within the middle sublayers of the SIMS structure. This is due to the relatively low flow rate (800 sccm) of O_2 and O_2^* was used. The Si doping during the growth was well controlled. However, the sub-layer thickness does influence the resolution of the SIMS data. In this work, the thicknesses of the sub-layers were 150-200 nm. While from our prior work[60], the thicknesses of SIMS sub-layers ranged between 200-400 nm, which provided much better resolution of Si doping depth profiles. Sufficient oxygen in gas phase enables the effective reaction of O_2 with C at the growth surface and thus suppresses the C incorporation in the grown films. In addition, with the similar flow rate of O_2 and O_2^*, there exists an obvious increase of H incorporation by using O_2^* as O precursor, indicating the effectiveness of introducing H by introducing H_2O in the precursor. In our previous study, using high-purity oxygen (99.9999%) resulted in similar H concentrations in the Si-doped and UID layer.[60] However, when O_2^* was used in this study, a significant increase in H concentration was observed in the Si-doped layers as compared to that of the UID layers. The higher H incorporation in the Si doped layer is likely related to the excessive H_2O or H radicals, potentially leading to the formation of a Si-H complex. Previous DFT calculations indicate that although Si_{Ga} and interstitial hydrogen (H_i), are energetically favorable, the Si-H complex is stable at cooling-down temperatures.[61] Prior study has also demonstrated that intentional hydrogenation can produce this Si-H complex in Ga_2O_3.[71] Thus, under a H-rich environment provided by H_2O, we believe that the formation of the Si-H complexes leads to the increased H concentration in the Si-doped layers. The relatively constant [Si] in the sub-layers with intentional Si doping indicates the insensitiveness of Si incorporation as the O_2 or O_2^* flow rate varies. The quantitative SIMS data indicate the significant impact of VI/III ratio on the background C incorporation in MOCVD β-Ga_2O_3, which in turn determines the compensation level in the grown films. With suppressed C

incorporation and low compensation, it is feasible to achieve low controllable doping even at fast growth rate conditions.

Figure 5 plots the room temperature electron mobility vs. carrier concentration for different series of β-Ga_2O_3 films grown at different conditions. All the samples were grown using TMGa, and the growth conditions were listed in Table 1 and Table 2. The plot also includes representative Hall data from our previous studies on β-Ga_2O_3 grown with TMGa and TEGa via MOCVD.[7, 11, 13] As shown in Figure 5, as O_2 (or O_2^*) flow rate increased from 800 to 2000 sccm, low controllable doping as low as 7 x10^{15} cm^{-3} was achieved with RT Hall mobility of 190 $cm^2/V{\cdot}s$ at a growth rate of 4.5 um/h, aligning closely with the record mobility value from β-Ga_2O_3 grown with a growth rate of 3 μm/h. The silane flow rates of sample #11 and #12 were 10 sccm, and 5 sccm, respectively. Comparing this silane flow rate with the total gas flow (>6500 sccm), this small modification of silane flow rate is not expected to impact the surface morphology. Therefore, the surface of sample #12 should be similar to that of the sample #11. With increased growth rates of 7 μm/h and 8.1 μm/h, electron concentration of 1.5 x10^{17} cm^{-3} with a RT Hall mobility of 93 $cm^2/V{\cdot}s$ and 6.2 x10^{17} cm^{-3} with a RT Hall mobility of 109 $cm^2/V{\cdot}s$ was also achieved. The doping levels of the samples in this study ranged from 7 x10^{15} cm^{-3} to 3.6 x10^{18} cm^{-3}. For the specific samples analyzed for surface morphology comparison (samples #1-4, 6, 7, 11, 13-16), the doping levels varied between 1.6 x10^{16} cm^{-3} and 3.1 x10^{18} cm^{-3}. Within this doping range, one should not expect significant variation on the surface morphologies. Even if the level of doping does influence the surface morphology, any resulting defects or surface roughness are expected to be uniformly distributed across the entire surface of the samples. Importantly, this study focuses on addressing the markedly large 3D features that are not due to doping.

In summary, MOCVD development of β-Ga_2O_3 films using TMGa as Ga precursor was demonstrated to achieve fast growth rate over 4.3 μm/h, smooth surface morphology, low controllable doping and high electron mobility. Systematic studies indicate that MOCVD growth conditions such as VI/III ratio, the use of O_2 (or O_2^*), and the selection of off-axis Ga_2O_3 substrates play important roles that determine the quality of the grown films. The use of O_2^* improved the surface morphologies with reduced size and density of 3D pyramid-shaped structural defects. β-Ga_2O_3 substrates with off-axis angles also provide a strategy to improve the surface morphologies of the thick β-Ga_2O_3 epitaxial films with fast growth rates. Quantitative SIMS characterization revealed the suppression of C incorporation with the increase of O_2 (or O_2^*) flow rates, which is particularly essential for developing thick β-Ga_2O_3 films. With optimal MOCVD growth conditions, high quality β-Ga_2O_3 films were achieved with fast growth rate (4.3 μm/h), low n-type doping (7 x10^{15} cm^{-3}), and high RT electron Hall mobility (190 $cm^2/V{\cdot}s$). Results from this work provide guidance on MOCVD development of high crystalline quality β-Ga_2O_3 films for vertical power electronics.

Acknowledgments

The authors acknowledge the financial support from the Air Force Office of Scientific Research FA9550-18-1-0479 (AFOSR, Dr. Ali Sayir), the National Science Foundation (Grant No. 2231026) and the Advanced Research Projects Agency-Energy (ARPA-E), U.S. Department of Energy, under Award Number DE-AR0001036.

Data Availability

The data that support the findings of this study are available from the corresponding author upon reasonable request.

References

[1] M. Higashiwaki, K. Sasaki, A. Kuramata, T. Masui, and S. Yamakoshi, Applied Physics Letters **100**(1), 013504 (2012).
[2] S. Yoshioka, H. Hayashi, A. Kuwabara, F. Oba, K. Matsunaga, and I. Tanaka, J. Phys.: Condens. Matter **19**(34), 346211 (2007).
[3] H. Peelaers, and C.G. Van De Walle, Physica Status Solidi (b) **252**(4), 828–832 (2015).
[4] Y. Kang, K. Krishnaswamy, H. Peelaers, and C.G. Van De Walle, J. Phys.: Condens. Matter **29**(23), 234001 (2017).
[5] J.B. Varley, J.R. Weber, A. Janotti, and C.G. Van De Walle, Applied Physics Letters **97**(14), 142106 (2010).
[6] C.H.-Y. MA Yan-Mei, Chin. Phys. Lett. **25**(5), 1603–1605 (2008).
[7] L. Meng, Z. Feng, A.F.M.A.U. Bhuiyan, and H. Zhao, Crystal Growth & Design **22**(6), 3896–3904 (2022).
[8] K. Goto, K. Konishi, H. Murakami, Y. Kumagai, B. Monemar, M. Higashiwaki, A. Kuramata, and S. Yamakoshi, Thin Solid Films **666**, 182–184 (2018).
[9] Y. Zhang, F. Alema, A. Mauze, O.S. Koksaldi, R. Miller, A. Osinsky, and J.S. Speck, APL Materials **7**(2), 022506 (2019).
[10] S. Rafique, L. Han, A.T. Neal, S. Mou, J. Boeckl, and H. Zhao, Physica Status Solidi (a) **215**(2), 1700467 (2018).
[11] Z. Feng, A.F.M. Anhar Uddin Bhuiyan, M.R. Karim, and H. Zhao, Applied Physics Letters **114**(25), 250601 (2019).
[12] F. Alema, G. Seryogin, A. Osinsky, and A. Osinsky, APL Materials **9**(9), 091102 (2021).
[13] Z. Feng, A.F.M.A.U. Bhuiyan, Z. Xia, W. Moore, Z. Chen, J.F. McGlone, D.R. Daughton, A.R. Arehart, S.A. Ringel, S. Rajan, and H. Zhao, Physica Status Solidi (RRL) – Rapid Research Letters **14**(8), 2000145 (2020).
[14] M.H. Wong, O. Bierwagen, R.J. Kaplar, and H. Umezawa, Journal of Materials Research **36**(23), 4601–4615 (2021).
[15] I. Friel, S.L. Clewes, H.K. Dhillon, N. Perkins, D.J. Twitchen, and G.A. Scarsbrook, Diamond and Related Materials **18**(5–8), 808–815 (2009).
[16] W. Saslow, T.K. Bergstresser, and M.L. Cohen, Phys. Rev. Lett. **16**(9), 354–356 (1966).
[17] M. Xu, D. Wang, K. Fu, D.H. Mudiyanselage, H. Fu, and Y. Zhao, Oxford Open Materials Science **2**(1), itac004 (2022).
[18] J. Y. Tsao, S. Chowdhury, M. A. Hollis, D. Jena, N. M. Johnson, K. A. Jones, R. J. Kaplar, S. Rajan, C. G. Van de Walle, E. Bellotti, C. L. Chua, R. Collazo, M. E. Coltrin, J. A. Cooper, K. R. Evans, S. Graham, T. A. Grotjohn, E. R. Heller, M. Higashiwaki, M. S. Islam, P. W. Juodawlkis, M. A. Khan, A. D. Koehler, J. H. Leach, U. K. Mishra, R. J. Nemanich, R. C. N. Pilawa-Podgurski, J. B. Shealy, Z. Sitar, M. J. Tadjer, A. F. Witulski, M. Wraback, J. A. Simmons, Adv. Electron. Mater., 4, 1600501 (2018).
[19] S. Roy, X. Zhang, A. B. Puthirath, A. Meiyazhagan, S. Bhattacharyya, M. M. Rahman, G. Babu, S. Susarla, S. K. Saju, M. K. Tran, L. M. Sassi, M. A. S. R. Saadi, J. Lai, O. Sahin, S. M. Sajadi, B. Dharmarajan, D. Salpekar, N. Chakingal, A. Baburaj, X. Shuai, A. Adumbumkulath, K. A. Miller, J. M. Gayle, A. Ajnsztajn, T. Prasankumar, V. V. J. Harikrishnan, V. Ojha, H. Kannan, A. Z. Khater, Z. Zhu, S. A. Iyengar, P. A. d. S. Autreto, E. F. Oliveira, G. Gao, A. G. Birdwell, M. R. Neupane, T. G. Ivanov, J. Taha-Tijerina, R. M.

Yadav, S. Arepalli, R. Vajtai, P. M. Ajayan, Structure, Properties and Applications of Two-Dimensional Hexagonal Boron Nitride. Adv. Mater., 33, 2101589 (2021).
[20] M. Higashiwaki, H. Murakami, Y. Kumagai, and A. Kuramata, Jpn. J. Appl. Phys. **55**(12), 1202A1 (2016).
[21] K. Sasaki, M. Higashiwaki, A. Kuramata, T. Masui, and S. Yamakoshi, Journal of Crystal Growth **378**, 591–595 (2013).
[22] C. Wang, J. Zhang, S. Xu, C. Zhang, Q. Feng, Y. Zhang, J. Ning, S. Zhao, H. Zhou, and Y. Hao, J. Phys. D: Appl. Phys. **54**(24), 243001 (2021).
[23] M.H. Wong, K. Goto, H. Murakami, Y. Kumagai, and M. Higashiwaki, IEEE Electron Device Lett. **40**(3), 431–434 (2019).
[24] E. Farzana, F. Alema, W.Y. Ho, A. Mauze, T. Itoh, A. Osinsky, and J.S. Speck, Applied Physics Letters **118**(16), 162109 (2021).
[25] K. Konishi, K. Goto, H. Murakami, Y. Kumagai, A. Kuramata, S. Yamakoshi, and M. Higashiwaki, Applied Physics Letters **110**(10), 103506 (2017).
[26] S. Kumar, H. Murakami, Y. Kumagai, and M. Higashiwaki, Appl. Phys. Express **15**(5), 054001 (2022).
[27] N. Allen, M. Xiao, X. Yan, K. Sasaki, M.J. Tadjer, J. Ma, R. Zhang, H. Wang, and Y. Zhang, IEEE Electron Device Lett. **40**(9), 1399–1402 (2019).
[28] X. Chen, F. Ren, S. Gu, and J. Ye, Photon. Res. **7**(4), 381 (2019).
[29] X. Hou, Y. Zou, M. Ding, Y. Qin, Z. Zhang, X. Ma, P. Tan, S. Yu, X. Zhou, X. Zhao, G. Xu, H. Sun, and S. Long, J. Phys. D: Appl. Phys. **54**(4), 043001 (2021).
[30] M.-Y. Tsai, O. Bierwagen, M.E. White, and J.S. Speck, Journal of Vacuum Science & Technology A: Vacuum, Surfaces, and Films **28**(2), 354–359 (2010).
[31] P. Vogt, A. Mauze, F. Wu, B. Bonef, and J.S. Speck, Appl. Phys. Express **11**(11), 115503 (2018).
[32] P. Vogt, F.V.E. Hensling, K. Azizie, C.S. Chang, D. Turner, J. Park, J.P. McCandless, H. Paik, B.J. Bocklund, G. Hoffman, O. Bierwagen, D. Jena, H.G. Xing, S. Mou, D.A. Muller, S.-L. Shang, Z.-K. Liu, and D.G. Schlom, APL Materials **9**(3), 031101 (2021).
[33] P. Mazzolini, A. Falkenstein, C. Wouters, R. Schewski, T. Markurt, Z. Galazka, M. Martin, M. Albrecht, and O. Bierwagen, APL Materials **8**(1), 011107 (2020).
[34] S. Rafique, L. Han, M.J. Tadjer, J.A. Freitas, N.A. Mahadik, and H. Zhao, Applied Physics Letters **108**(18), 182105 (2016).
[35] S. Rafique, L. Han, A.T. Neal, S. Mou, M.J. Tadjer, R.H. French, and H. Zhao, Applied Physics Letters **109**(13), 132103 (2016).
[36] S. Rafique, M.R. Karim, J.M. Johnson, J. Hwang, and H. Zhao, Applied Physics Letters **112**(5), 052104 (2018).
[37] Y. Zhang, Z. Feng, M.R. Karim, and H. Zhao, Journal of Vacuum Science & Technology A: Vacuum, Surfaces, and Films **38**(5), 050806 (2020).
[38] K. Matsuzaki, H. Hiramatsu, K. Nomura, H. Yanagi, T. Kamiya, M. Hirano, and H. Hosono, Thin Solid Films **496**(1), 37–41 (2006).
[39] K.D. Leedy, K.D. Chabak, V. Vasilyev, D.C. Look, J.J. Boeckl, J.L. Brown, S.E. Tetlak, A.J. Green, N.A. Moser, A. Crespo, D.B. Thomson, R.C. Fitch, J.P. McCandless, and G.H. Jessen, Applied Physics Letters **111**(1), 012103 (2017).
[40] F.B. Zhang, K. Saito, T. Tanaka, M. Nishio, and Q.X. Guo, Journal of Crystal Growth **387**, 96–100 (2014).

[41] H. Murakami, K. Nomura, K. Goto, K. Sasaki, K. Kawara, Q.T. Thieu, R. Togashi, Y. Kumagai, M. Higashiwaki, A. Kuramata, S. Yamakoshi, B. Monemar, and A. Koukitu, Appl. Phys. Express **8**(1), 015503 (2015).
[42] J.H. Leach, K. Udwary, J. Rumsey, G. Dodson, H. Splawn, and K.R. Evans, APL Materials **7**(2), 022504 (2019).
[43] Y. Zhang, F. Alema, A. Mauze, O.S. Koksaldi, R. Miller, A. Osinsky, and J.S. Speck, APL Materials **7**(2), 022506 (2019).
[44] L. Meng, Z. Feng, A.F.M.A.U. Bhuiyan, and H. Zhao, Crystal Growth & Design **22**(6), 3896–3904 (2022).
[45] Z. Feng, A.F.M.A.U. Bhuiyan, N.K. Kalarickal, S. Rajan, and H. Zhao, Applied Physics Letters **117**(22), 222106 (2020).
[46] A. Hernandez, M.M. Islam, P. Saddatkia, C. Codding, P. Dulal, S. Agarwal, A. Janover, S. Novak, M. Huang, T. Dang, M. Snure, and F.A. Selim, Results in Physics **25**, 104167 (2021).
[47] D. Gogova, M. Ghezellou, D.Q. Tran, S. Richter, A. Papamichail, J.U. Hassan, A.R. Persson, P.O.Å. Persson, O. Kordina, B. Monemar, M. Hilfiker, M. Schubert, P.P. Paskov, and V. Darakchieva, AIP Advances **12**(5), 055022 (2022).
[48] Z. Li, T. Jiao, J. Yu, D. Hu, Y. Lv, W. Li, X. Dong, B. Zhang, Y. Zhang, Z. Feng, G. Li, and G. Du, Vacuum **178**, 109440 (2020).
[49] T. Jiao, Z. Li, W. Chen, X. Dong, Z. Li, Z. Diao, Y. Zhang, and B. Zhang, Coatings **11**(5), 589 (2021).
[50] M. Higashiwaki, K. Sasaki, K. Goto, K. Nomura, Q.T. Thieu, R. Togashi, H. Murakami, Y. Kumagai, B. Monemar, A. Koukitu, A. Kuramata, and S. Yamakoshi, "Ga2O3 Schottky barrier diodes with n$^{\&\#x2212;}$-Ga2O3 drift layers grown by HVPE," in 2015 73rd Annual Device Research Conference (DRC), (IEEE, Columbus, OH, USA, 2015), pp. 29–30.
[51] M. Higashiwaki, "β-Ga2O3 material properties, growth technologies, and devices: a review," AAPPS Bull. **32**(1), 3 (2022).
[52] H. Sheoran, J.K. Kaushik, and R. Singh, "Study of electrical characteristics of high quality Pt SBDs fabricated on HVPE-Grown β-Ga2O3 epilayers in a wide temperature range (80–525 K)," Materials Science in Semiconductor Processing **165**, 107606 (2023).
[53] C. Wang, J. Zhang, S. Xu, C. Zhang, Q. Feng, Y. Zhang, J. Ning, S. Zhao, H. Zhou, and Y. Hao, "Progress in state-of-the-art technologies of Ga $_2$ O $_3$ devices," J. Phys. D: Appl. Phys. **54**(24), 243001 (2021).
[54] M.H. Wong, and M. Higashiwaki, "Vertical β -Ga_2O_3 Power Transistors: A Review," IEEE Trans. Electron Devices **67**(10), 3925–3937 (2020).
[55] Y. Oshima, E.G. Víllora, Y. Matsushita, S. Yamamoto, and K. Shimamura, "Epitaxial growth of phase-pure ε-Ga2O3 by halide vapor phase epitaxy," Journal of Applied Physics **118**(8), 085301 (2015).
[56] F. Alema, B. Hertog, A. Osinsky, P. Mukhopadhyay, M. Toporkov, and W.V. Schoenfeld, Journal of Crystal Growth **475**, 77–82 (2017).
[57] G. Seryogin, F. Alema, N. Valente, H. Fu, E. Steinbrunner, A.T. Neal, S. Mou, A. Fine, and A. Osinsky, Applied Physics Letters **117**(26), 262101 (2020).
[58] C.A. Larsen, N.I. Buchan, S.H. Li, and G.B. Stringfellow, Journal of Crystal Growth **102**(1–2), 103–116 (1990).
[59] P.W. Lee, T.R. Omstead, D.R. McKenna, and K.F. Jensen, Journal of Crystal Growth **85**(1–2), 165–174 (1987).
[60] L. Meng, A.F.M.A.U. Bhuiyan, and H. Zhao, Applied Physics Letters **122**(23), 232106 (2023).

[61] S. Mu, M. Wang, J.B. Varley, J.L. Lyons, D. Wickramaratne, and C.G. Van De Walle, Phys. Rev. B **105**(15), 155201 (2022).
[62] L. Meng, A.F.M.A.U. Bhuiyan, Z. Feng, H.-L. Huang, J. Hwang, and H. Zhao, Journal of Vacuum Science & Technology A **40**, 062706
[63] S. Bin Anooz, R. Grüneberg, C. Wouters, R. Schewski, M. Albrecht, A. Fiedler, K. Irmscher, Z. Galazka, W. Miller, G. Wagner, J. Schwarzkopf, and A. Popp, Appl. Phys. Lett. **116**, 182106 (2020).
[64] G. Wagner, M. Baldini, D. Gogova, M. Schmidbauer, R. Schewski, M. Albrecht, Z. Galazka, D. Klimm, and R. Fornari, Phys. Status Solidi A **211**, 27 (2014).
[65] D. Gogova, G. Wagner, M. Baldini, M. Schmidbauer, K. Irmscher, R. Schewski, Z. Galazka, M. Albrecht, and R. Fornari, J. Cryst. Growth **401**, 665 (2014).
[66] A. Fiedler, R. Schewski, M. Baldini, Z. Galazka, G. Wagner, M. Albrecht, and K. Irmscher, J. Appl. Phys. **122**, 165701 (2017).
[67] R. Schewski, M. Baldini, K. Irmscher, A. Fiedler, T. Markurt, B. Neuschulz, T. Remmele, T. Schulz, G. Wagner, Z. Galazka, and M. Albrecht, J. Appl. Phys. **120**, 225308 (2016).
[68] R. Schewski, K. Lion, A. Fiedler, C. Wouters, A. Popp, S.V. Levchenko, T. Schulz, M. Schmidbauer, S. Bin Anooz, R. Grüneberg, Z. Galazka, G. Wagner, K. Irmscher, M. Scheffler, C. Draxl, and M. Albrecht, APL Mater. **7**, 022515 (2019).
[69] F. Alema, Y. Zhang, A. Mauze, T. Itoh, J. S. Speck, B. Hertog, and A. Osinsky, AIP Advances, 10(8), 085002, (2020).
[70] G. Wagner, M. Baldini, D. Gogova, M. Schmidbauer, R. Schewski, M. Albrecht, Z. Galazka, D. Kimm, and R. Fomari, Physica Status Solidi (a) 211, 27, (2014).
[71] A. Venzie, A. Portoff, C. Fares, M. Stavola, W. Beall Fowler, F. Ren, S. Pearton, Appl. Phys. Letts. 119, 062109 (2021).

Table Captions

Table 1. Summary of the β-Ga_2O_3 epi-films grown on (010) semi-insulating Fe-doped β-Ga_2O_3 substrates with different growth parameters and the corresponding characteristics: O_2 with high purity (≥ 99.9999 %) or O_2^* with 10 ppm of [H_2O], TMGa molar flow rate, VI/III molar ratios, oxygen flow rate, carrier gas (Ar) flow rate, growth duration, film thickness, electron concentration, and RT electron Hall mobility. The chamber pressure and growth temperature were fixed at 60 torr and 950 ℃, respectively.

Table 2. Overview of the β-Ga_2O_3 epi-films grown on 2º off-axis β-Ga_2O_3 substrates under various growth conditions and corresponding characteristics: O_2 with high purity (≥ 99.9999 %) or O_2^* with 10 ppm of [H_2O], TMGa molar flow rate, VI/III ratios, oxygen flow rate, carrier gas (Ar) flow rate, growth duration, film thickness, electron concentration, and RT electron Hall mobility. The chamber pressure and growth temperature were fixed at 60 torr and 950 ℃, respectively.

Figure Captions

Figure 1. Surface view in optical microscopic, FESEM, and AFM images of β-Ga_2O_3 epi-films grown on (010) semi-insulating Fe-doped β-Ga_2O_3 substrates with O_2 or O_2^*: (a) optical, (c, e) FESEM, (g) AFM images with O_2 (Sample #2) and (b) optical, (d, f) FESEM, and (h) AFM images with O_2^* (Sample #11). The TMGa molar flow rate, chamber pressure, growth temperature, and growth duration were set at 87 μmol/min, 60 torr, 950 ℃, and 84 mins, respectively.

Figure 2. Surface view in optical microscopic, FESEM, and AFM images of β-Ga_2O_3 epi-films grown on 2º off-cut and on-axis (010) semi-insulating β-Ga_2O_3 substrates under varied growth conditions. The chamber pressure and growth temperature were set at 60 Torr and 950 ℃, respectively.

Figure 3. Surface view in optical microscopic, FESEM, and AFM images of β-Ga_2O_3 epi-films grown on (010) Fe-doped β-Ga_2O_3 substrates with various VI/III ratios (308 – 1155). The chamber pressure and growth temperature were fixed with 60 Torr and 950 ℃, respectively.

Figure 4. (a) Schematic cross-section diagram of the SIMS sample composed of Si-doped β-Ga_2O_3 sub-layers grown with O_2^* vs. O_2, and for each case, the β-Ga_2O_3 sub-layers were grown with fixed TMGa molar flow rate of 87 μmol/min with different O_2 (or O_2^*) flow rate of 2000 (i), 1500 (ii) and 800 (iii) sccm. These Si-doped sub-layers were separated by UID β-Ga_2O_3 sub-layers which were grown under the same growth condition as the adjacent layer but without Si-doping. (b) Quantitative SIMS impurity depth profiles for C, H, and Si for the designed SIMS sample. Detection limit for [Si]: 2×10^{15} cm^{-3}, [C]: 5×10^{16} cm^{-3}, and [H]: 5×10^{16} cm^{-3}.

Figure 5. Comparison of the RT Hall mobility data for (010) β-Ga_2O_3 epi-films grown using TMGa with fast growth rates (4.3 - 8.1 μm/h) as a function of the electron concentration from this work, and previously reported data from MOCVD grown (010) β-Ga_2O_3 thin films.

Table 1.

Sample ID	Oxygen purity	TMGa molar flow rate (μmol/min)	Oxygen flow rate (sccm)	VI/III ratios	Silane molar flow rate (nmol/min)	Growth duration (min.)	Film thickness (μm)	Electron concentration (cm^{-3})	Hall mobility ($cm^2/V \cdot s$)
#1	O_2	116	800	308	40	60	7	1.8×10^{18}	11
#2	O_2	87	2000	1026	0.08	84	6.3	1.4×10^{16}	180
#3	O_2^*	116	800	308	40	60	7	1.5×10^{17}	93
#4	O_2^*	116	1000	385	40	60	8.1	6.2×10^{17}	109
#5	O_2^*	116	1500	577	40	60	7	3.6×10^{18}	92
#6	O_2^*	116	3000	1155	40	60	6	3×10^{18}	117
#7	O_2^*	87	2000	1026	10.1	84	6.3	1.3×10^{18}	110
#8	O_2^*	87	2000	1026	4	84	6.3	5.6×10^{17}	129
#9	O_2^*	87	2000	1026	1.7	84	6.3	2.3×10^{17}	147
#10	O_2^*	87	2000	1026	0.44	84	6.3	5.8×10^{16}	169
#11	O_2^*	87	2000	1026	0.08	84	6.3	1.3×10^{16}	185
#12	O_2^*	87	2000	1026	0.03	84	6.3	7×10^{15}	190
#13	O_2^*	87	2000	1026	22	134	9.6	2.8×10^{18}	120

Table 2.

Sample ID	Oxygen purity	TMGa molar flow rate (μmol/min)	Oxygen flow rate (sccm)	VI/III ratios	Silane molar flow rate (nmol/min)	Growth duration (min.)	Film thickness (μm)	Electron concentration (cm^{-3})	Hall mobility ($cm^2/V \cdot s$)
#14	O_2	116	800	308	40	60	7	-	-
#15	O_2^*	116	1000	385	0.08	60	8.1	3×10^{18}	95
#16	O_2^*	87	2000	1026	24	134	9.6	2.5×10^{18}	108

Figure 1.

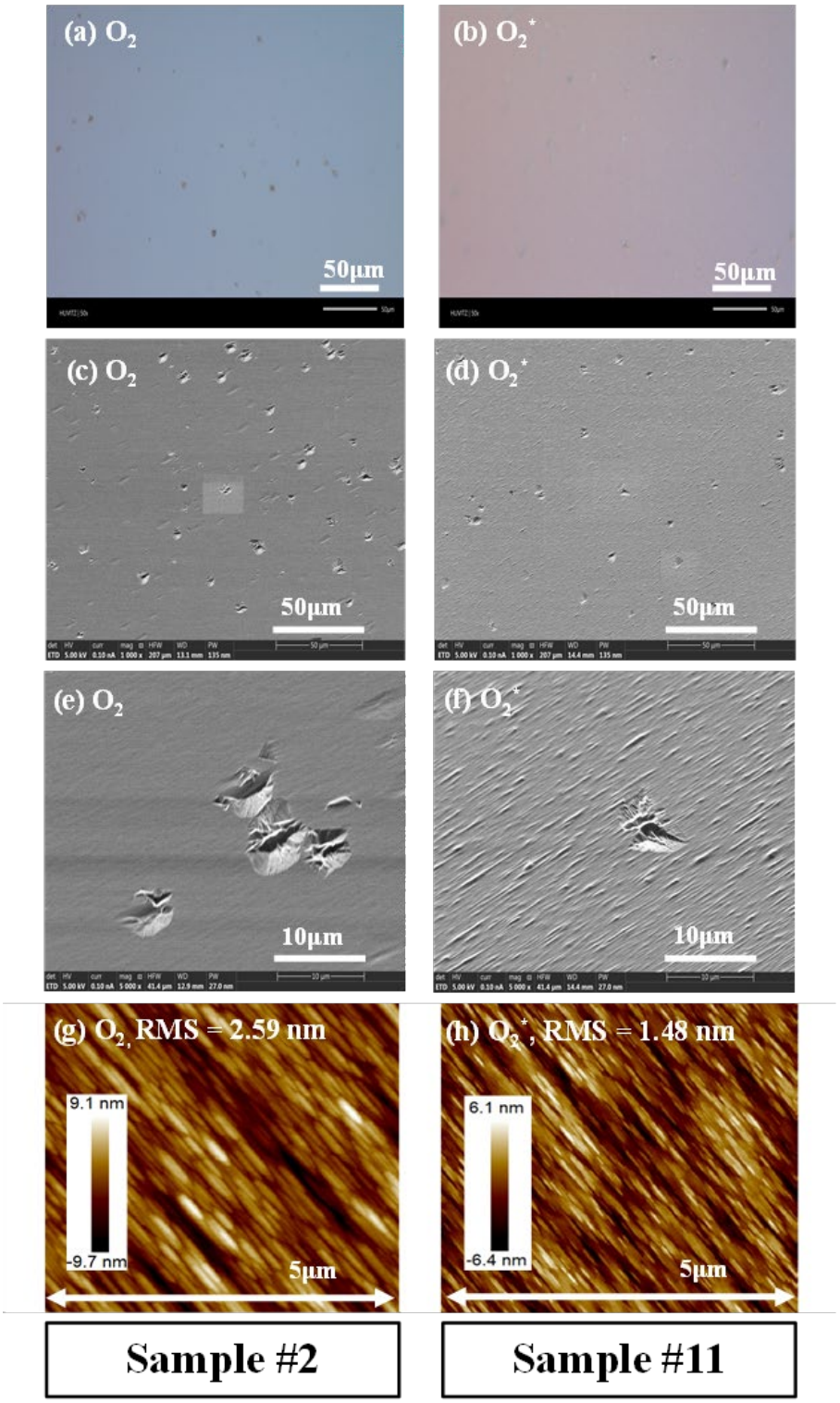
(a) O_2
50µm
(b) O_2^+
50µm
(c) O_2
50µm
(d) O_2^+
50µm
(e) O_2
10µm
(f) O_2^+
10µm
(g) O_2, RMS = 2.59 nm
9.1 nm
-9.7 nm
5µm
(h) O_2^+, RMS = 1.48 nm
6.1 nm
-6.4 nm
5µm
Sample #2
Sample #11

Figure 2.

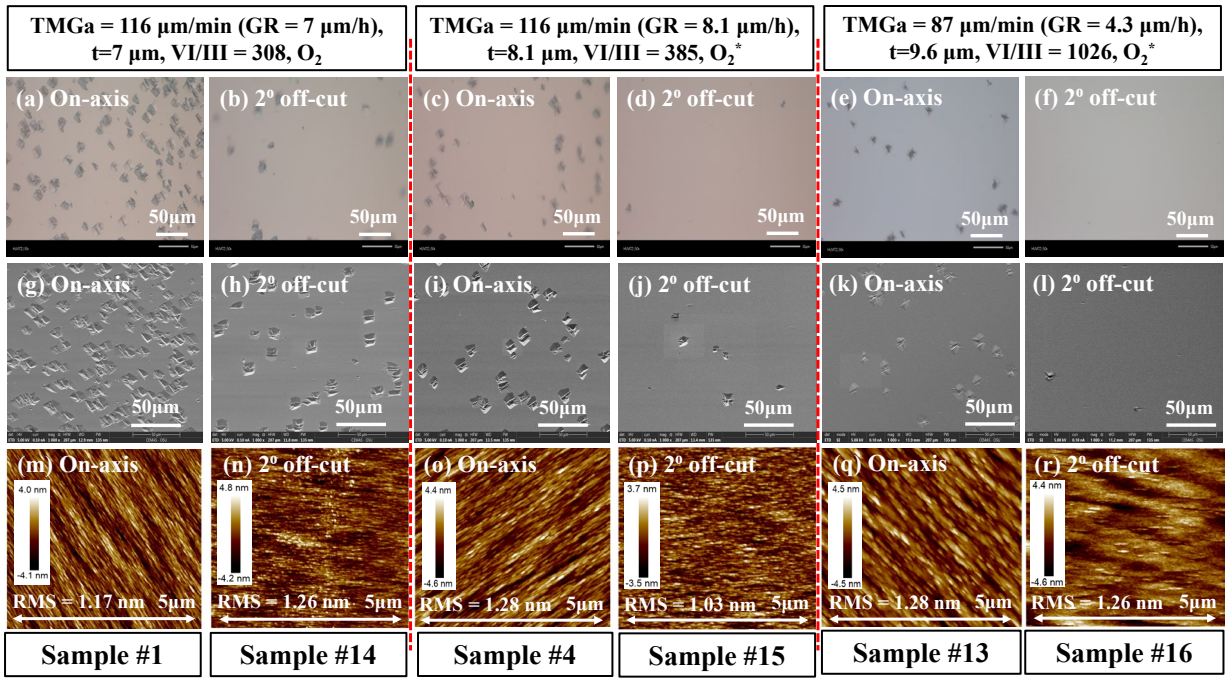
TMGa = 116 µm/min (GR = 7 µm/h), t=7 µm, VI/III = 308, O2
TMGa = 116 µm/min (GR = 8.1 µm/h), t=8.1 µm, VI/III = 385, O2*
TMGa = 87 µm/min (GR = 4.3 µm/h), t=9.6 µm, VI/III = 1026, O2*
(a) On-axis
(b) 2º off-cut
(c) On-axis
(d) 2º off-cut
(e) On-axis
(f) 2º off-cut
(g) On-axis
(h) 2º off-cut
(i) On-axis
(j) 2º off-cut
(k) On-axis
(l) 2º off-cut
50µm
(m) On-axis
(n) 2º off-cut
(o) On-axis
(p) 2º off-cut
(q) On-axis
(r) 2º off-cut
RMS = 1.17 nm 5µm
RMS = 1.26 nm 5µm
RMS = 1.28 nm 5µm
RMS = 1.03 nm 5µm
RMS = 1.28 nm 5µm
RMS = 1.26 nm 5µm
Sample #1
Sample #14
Sample #4
Sample #15
Sample #13
Sample #16

Figure 3.

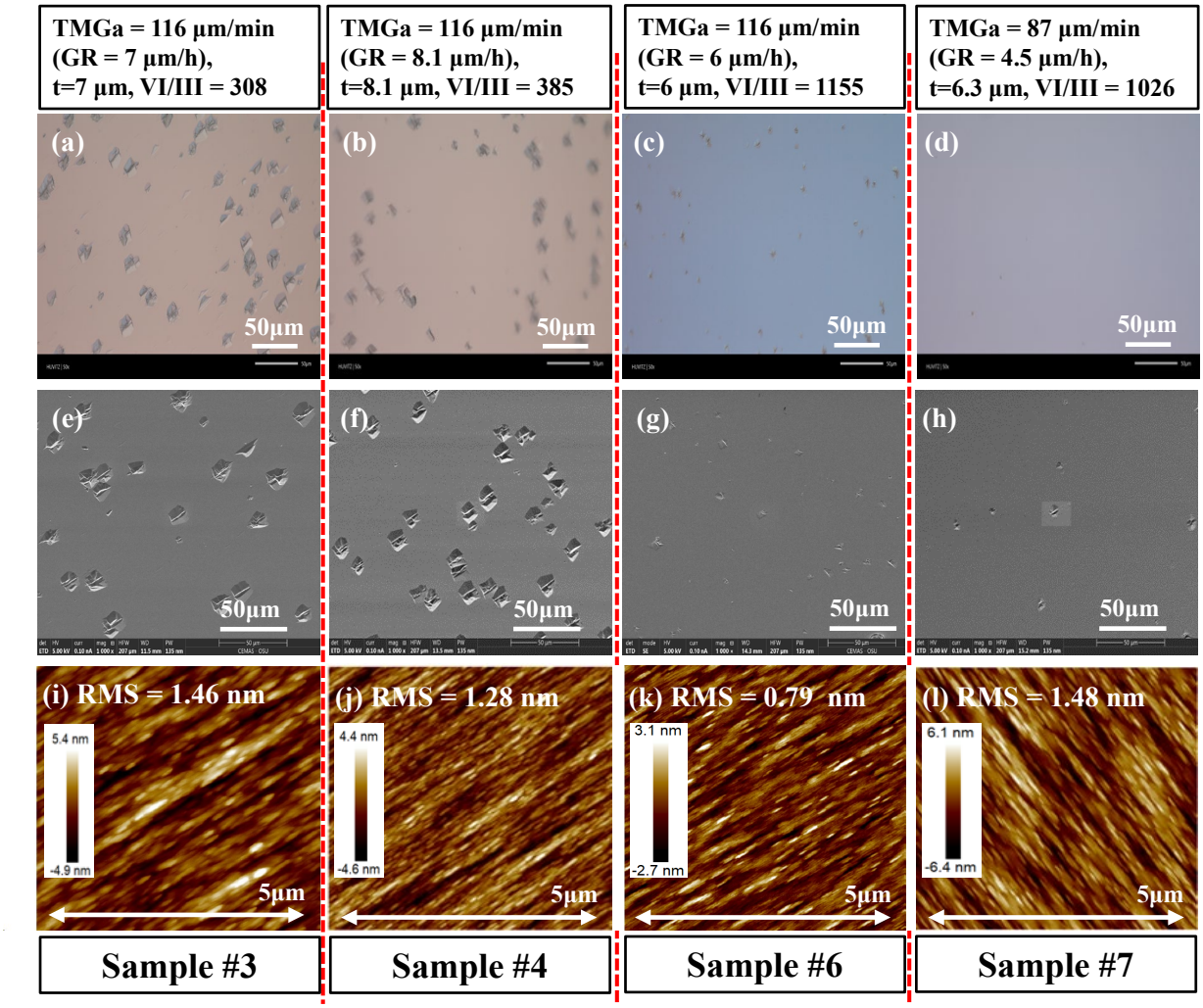
TMGa = 116 µm/min (GR = 7 µm/h), t=7 µm, VI/III = 308
TMGa = 116 µm/min (GR = 8.1 µm/h), t=8.1 µm, VI/III = 385
TMGa = 116 µm/min (GR = 6 µm/h), t=6 µm, VI/III = 1155
TMGa = 87 µm/min (GR = 4.5 µm/h), t=6.3 µm, VI/III = 1026
(a)
(b)
(c)
(d)
(e)
(f)
(g)
(h)
50µm
(i) RMS = 1.46 nm
(j) RMS = 1.28 nm
(k) RMS = 0.79 nm
(l) RMS = 1.48 nm
5.4 nm
-4.9 nm
4.4 nm
-4.6 nm
3.1 nm
-2.7 nm
6.1 nm
-6.4 nm
5µm
Sample #3
Sample #4
Sample #6
Sample #7

Figure 4.

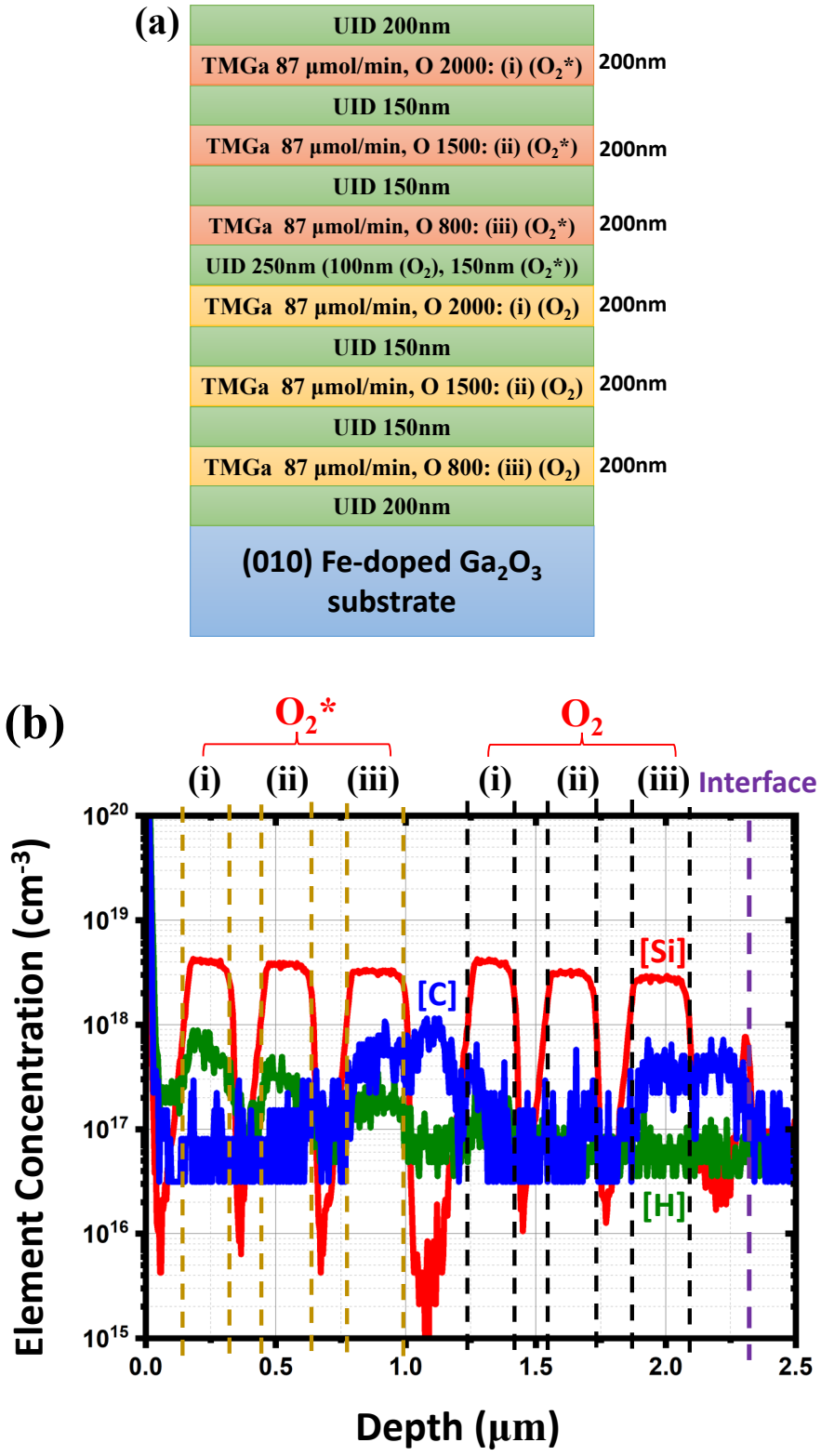
(a)
UID 200nm
TMGa 87 µmol/min, O 2000: (i) (O2*)
200nm
UID 150nm
TMGa 87 µmol/min, O 1500: (ii) (O2*)
200nm
UID 150nm
TMGa 87 µmol/min, O 800: (iii) (O2*)
200nm
UID 250nm (100nm (O2), 150nm (O2*))
TMGa 87 µmol/min, O 2000: (i) (O2)
200nm
UID 150nm
TMGa 87 µmol/min, O 1500: (ii) (O2)
200nm
UID 150nm
TMGa 87 µmol/min, O 800: (iii) (O2)
200nm
UID 200nm
(010) Fe-doped Ga2O3 substrate
(b)
O2*
O2
(i)
(ii)
(iii)
(i)
(ii)
(iii)
Interface
[Si]
[C]
[H]
Element Concentration (cm-3)
Depth (µm)

Figure 5.

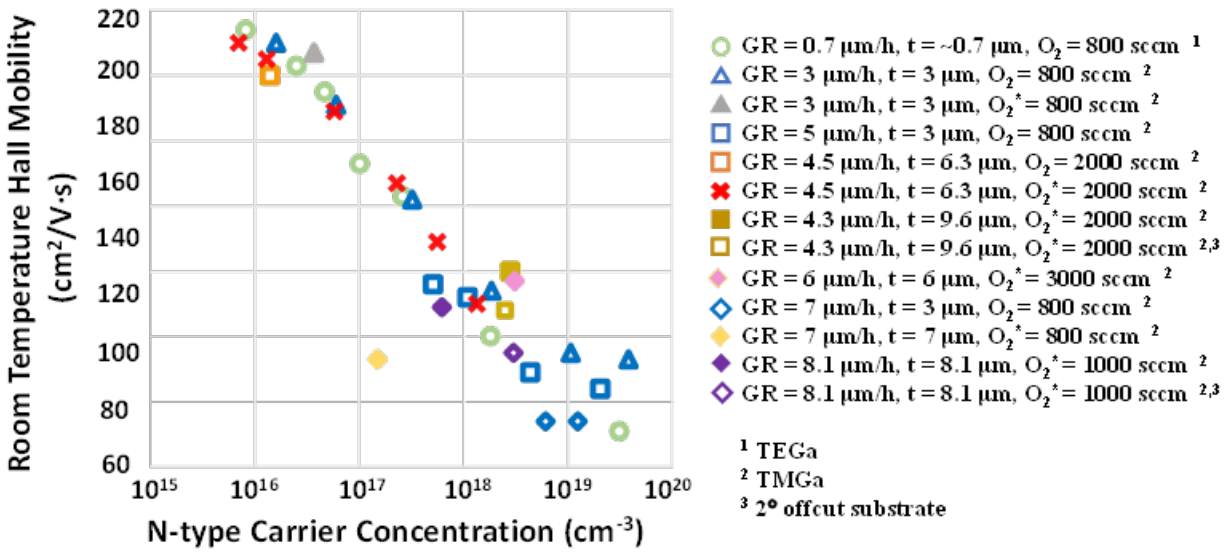
Room Temperature Hall Mobility (cm²/V·s)
220
200
180
160
140
120
100
80
60
10¹⁵
10¹⁶
10¹⁷
10¹⁸
10¹⁹
10²⁰
N-type Carrier Concentration (cm⁻³)
GR = 0.7 µm/h, t = ~0.7 µm, O2 = 800 sccm 1
GR = 3 µm/h, t = 3 µm, O2 = 800 sccm 2
GR = 3 µm/h, t = 3 µm, O2* = 800 sccm 2
GR = 5 µm/h, t = 3 µm, O2 = 800 sccm 2
GR = 4.5 µm/h, t = 6.3 µm, O2 = 2000 sccm 2
GR = 4.5 µm/h, t = 6.3 µm, O2* = 2000 sccm 2
GR = 4.3 µm/h, t = 9.6 µm, O2* = 2000 sccm 2
GR = 4.3 µm/h, t = 9.6 µm, O2* = 2000 sccm 2,3
GR = 6 µm/h, t = 6 µm, O2* = 3000 sccm 2
GR = 7 µm/h, t = 3 µm, O2 = 800 sccm 2
GR = 7 µm/h, t = 7 µm, O2* = 800 sccm 2
GR = 8.1 µm/h, t = 8.1 µm, O2* = 1000 sccm 2
GR = 8.1 µm/h, t = 8.1 µm, O2* = 1000 sccm 2,3
1 TEGa
2 TMGa
3 2° offcut substrate